Збірник наукових праць. Галузеве машинобудування, будівництво
Academic journal. Industrial Machine Building, Civil Engineering
http://journals.nupp.edu.ua/znp
https://doi.org/10.26906/znp.2025.65.4210

UDC 624.012

Olena Petrova
O.M. Beketov National University of Urban Economy in Kharkiv
https://orcid.org/0000-0003-0683-9694

Vladyslav Tenesesku
O.M. Beketov National University of Urban Economy in Kharkiv
https://orcid.org/0000-0002-8168-7224

Dmytro Petrenko
O.M. Beketov National University of Urban Economy in Kharkiv
https://orcid.org/0000-0002-8168-7224

Oleksii Buldakov
O.M. Beketov National University of Urban Economy in Kharkiv
https://orcid.org/0009-0002-4663-7392

Stress-Strain State Analysis of a Shallow Spherical Shell Fabricated Using 3DCP

Abstract. Experimental and numerical investigations of the stress–strain behavior and load-bearing capacity of a shallow spherical concrete shell fabricated using extrusion-based 3D printing are presented. The shell with a plan dimension of 2.2 × 2.2 m was subjected to quasi-uniform stepwise loading using sandbags. The maximum applied distributed load reached 13.74 kN/m², and the measured vertical deflections did not exceed 0.235 mm, indicating high structural stiffness. A three-dimensional nonlinear finite element model was developed in LS-DYNA to simulate the experimental behavior and to predict the ultimate load-bearing capacity, since it was not reached experimentally. It was found that failure of the 3D-printed shell occurs under a uniformly distributed load of 228.4 kN/m², which corresponds to a total load of 67.8 t. The numerical results showed good agreement with the experimental data, with discrepancies within 17%. The proposed experimental–numerical approach confirms the structural efficiency and feasibility of 3D-printed concrete shells for load-bearing applications.

Keywords: 3D-printed shell, experimental study, stress–strain state, 3D concrete printing, load-bearing capacity.

*Corresponding author E-mail: Vladislav.Tenesesku@kname.edu.ua

Received: 30.10.2025 Accepted: 18.11.2025 Published: 26.12.2025

Introduction.

The current advancement in the theory and practice of reinforced concrete shell design is driven by the integration of high-fidelity numerical methods, experimental validation, and emerging construction technologies. Classical analytical formulations based on thin shell theory are increasingly supplemented by three-dimensional finite element modeling, enabling the consideration of complex geometries, layered material behavior, and physical as well as geometric nonlinearities. These approaches are now widely applied not only to conventional reinforced concrete shells but also to structural systems produced using additive manufacturing. In contemporary research, numerical models are systematically verified through laboratory or full-scale experimental testing, thereby ensuring the reliability of performance predictions.

Experimental methodologies have evolved significantly over the past decade. In addition to conventional loading systems based on hydraulic actuators, hydrostatic loading techniques are increasingly employed to reproduce quasi-uniform pressure fields on curved surfaces, simulating snow, water, or soil loads. Advanced measurement techniques, including digital image correlation, high-resolution displacement sensors, and multi-point monitoring systems, enable full-field deformation and crack pattern assessment. Recent experimental studies confirm that thin shells with lightweight internal structures or composite reinforcement exhibit high spatial stiffness and are capable of sustaining substantial loads.

A rapidly developing research domain is associated with shell and shell-like concrete elements fabricated using extrusion-based 3D printing [1]. 3D-printed

cementitious materials exhibit pronounced anisotropy and interlayer weak interfaces [2–4], which strongly affect their structural response under compression, bending, and combined stress states. Shell geometries such as domes, vaults, and arches, when properly designed, primarily operate through membrane compression mechanisms, while bending stresses are localized near supports, boundaries, openings, and geometric discontinuities. This characteristic is particularly relevant for 3D concrete printing, where the integration of conventional reinforcement is technologically challenging [5]. Consequently, compression-dominated shell forms represent the most rational initial applications for load-bearing 3D-printed structures.

Recent studies have demonstrated the effectiveness of composite solutions combining 3D-printed cementitious layers with FRP substrates [6, 7], reinforced concrete infill, or steel and polymer fibers [8]. These hybrid systems exhibit enhanced load-bearing capacity, improved crack control, and increased energy dissipation at failure. Furthermore, technological investigations have confirmed the feasibility of printing spatially curved shell forms, including domes, variable-curvature shells, and thin panels, without traditional formwork or with minimal temporary support. In this context, the present study focuses on the experimental evaluation of the deformability of a 3D-printed concrete roof shell and on the numerical prediction of its ultimate load-bearing capacity, highlighting the structural potential of additive manufacturing for shell applications.

The problem of reproducing a uniformly distributed load on curved shell surfaces under laboratory conditions remains technically challenging. An analysis of existing experimental research indicates that most studies are conducted on small-scale specimens, which significantly simplifies testing procedures but limits the representativeness of the results for real-scale structures.

A comprehensive experimental methodology was proposed for long reinforced concrete cylindrical shells to evaluate their stress–strain state, load-bearing capacity, and crack resistance in [9]. A specialized test rig was developed, and eight shell specimens were fabricated, including four reinforced concrete and four steel fiber–reinforced concrete models (1% by volume). The specimens had identical length and curvature radius, while the thickness and edge element dimensions varied. Loading was applied by hydraulic jacks as a vertically distributed force along four longitudinal strips on the shell surface, with pinned supports at the corners. Deformations were recorded using dial gauges and strain gauges, and the ultimate load was defined as the load at which the shell lost its load-bearing capacity. The proposed methodology was shown to be universal and suitable for further research.

Experimental investigations of small-scale fiber-reinforced concrete dome shells were presented in [10]. The authors tested 21 dome specimens produced with different fiber types (industrial steel, recycled synthetic, and alternative fibers) and one reference plain concrete specimen. The domes were spherical thick-walled shells and were subjected to concentrated compressive loading at the crown using a hydraulic jack until failure. Load–deflection relationships and crack characteristics were obtained. The results demonstrated that fiber reinforcement significantly increased the load-bearing and deformation capacity of the domes and that recycled and alternative fibers can effectively replace conventional steel fibers while providing improved crack resistance and ductile behavior.

An innovative composite thin shell produced using extrusion-based 3D concrete printing and an FRP substrate was proposed in [11]. In this system, a flat FRP sheet serves as a permanent formwork and lower reinforcement layer, onto which a fast-hardening fiber-cement material is deposited by 3D printing. Experimental specimens were tested under bending and concentrated loading, and the results were compared with nonlinear finite element simulations in ABAQUS. The composite shell exhibited a significant increase in load-bearing capacity – approximately 53% compared with a conventional reinforced concrete shell. The dominant failure mechanism was peeling of the printed concrete layer from the FRP substrate after crack development.

López et al. [12] introduced a composite shell construction method combining a thin brick tile vault used as permanent formwork with a cast reinforced concrete layer. Two full-scale doubly curved “sail” domes were constructed and tested under static distributed loading until collapse. Artificial distributed loads were applied to simulate uniform surface pressure. Deflections, crack development, and failure mechanisms were recorded, and a finite element model was calibrated using the experimental data. The domes exhibited high load-bearing capacity and ductile collapse behavior, forming classical hinge mechanisms consistent with shell theory.

Hydrostatic loading of shell structures was investigated by Emelianova and Lobanova [13], who studied thin-walled reinforced concrete cylindrical tanks under internal water pressure. Small-scale models were tested by filling them with water until cracking and ultimate limit states were reached. The influence of wall–base connection conditions and external stiffening rings was analyzed, and an analytical method of successive approximations was validated against the experimental results.

An experimental and numerical study of a reinforced concrete spherical shell with a hollow internal structure was presented in [14]. The three-layer shell, incorporating an EPS core and diagonal stiffening ribs, was loaded hydrostatically using a cellular water basin to simulate uniformly distributed snow loading. The experimental results showed maximum deflections of up to 0.7 mm and were in good agreement with finite element simulations in ANSYS, confirming the accuracy of the adopted numerical model.

Despite the significant progress demonstrated in these studies, several challenges remain unresolved, including the limited number of full-scale experiments,

the absence of standardized design approaches for 3D-printed shell structures, and the difficulty of accounting for material anisotropy and printing-induced defects in engineering analyses. These gaps indicate the need for further experimental–numerical research on full-scale 3D-printed shell systems under distributed loading.

Problem statement.

The object of this study is a shallow spherical concrete roof shell fabricated using extrusion-based 3D printing. The shell has a diameter of 2.2 m, a rise of 0.3 m, and an average thickness of 80 mm. The support ring is reinforced with 2Ø10 A500C steel bars, and lifting loops are provided along all four sides to facilitate transportation and installation. The fabrication procedure is described in [15], and the general configuration of the specimen is shown in Fig. 1. The physical and mechanical properties of the printed material were obtained from laboratory tests on specimens produced using the same layered extrusion technique and mixture composition, as reported in [16, 17].

The shell was initially designed with a nominal thickness of 40 mm; however, post-fabrication 3D scanning (Leica RTC360) and point-cloud processing revealed a significant deviation from the design geometry. The measured thickness was approximately 80 mm, which is attributed to (i) geometric inaccuracies of the manually fabricated foam support form relative to the digital model and (ii) technological constraints of the printing process, including fixed nozzle paths at constant elevations, vertical material extrusion, and overlap of layers on the curved formwork surface. These factors resulted in a systematic increase in shell thickness, indicating that accurate digital modeling is critical for the production of shell and dome elements.

The aim of the study is to experimentally determine deformability of a 3D-printed concrete shell under quasi-uniformly distributed static loading and to numerically predict its ultimate capacity.

The research focus is the stress–strain response of the shell subjected to quasi-uniform static loads.

The objectives of this study are:

- to review current experimental approaches for reinforced concrete and 3D-printed shell structures;
- to experimentally quantify deflections and strains at characteristic locations of the shell;
- to develop and verify a three-dimensional finite element model using the experimental results;
- to investigate crack formation, failure mechanisms, and ultimate limit states of the shell.

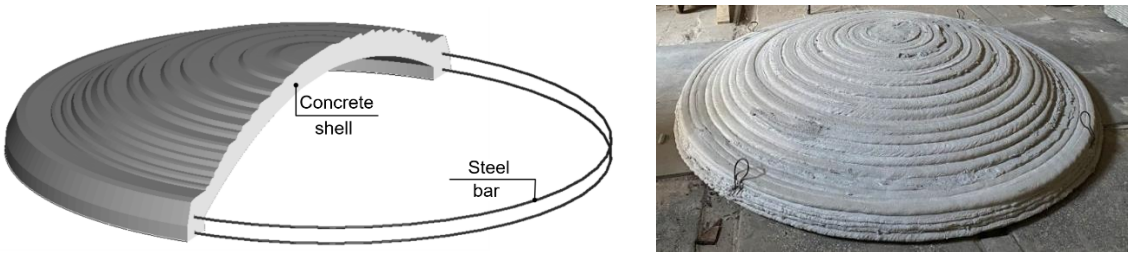

a) *b)*

Figure 1 – General view of the 3DCP shell: a) - schematic representation, b) - actual specimen

Main material and results.

Loading system. Prior to loading, the shell was visually inspected to confirm the absence of initial defects, and all measuring devices were zeroed.

To generate a quasi-uniformly distributed load, sandbags filled with washed sand were selected. Although full-scale shell tests using hydrostatic loading have been reported in the literature – particularly in the works of Grebenchuk [14], where cellular water basins of different sizes were used to simulate uniform pressure [18] – this approach was not adopted due to its high cost and technical limitations. In addition, the expected failure load of the shell would require an excessively high water column. Since the objective of the study was to investigate the shell under distributed loading representative of roof action, the use of hydraulic jacks and concentrated forces was also excluded.

The load was therefore applied by placing sandbags on the shell surface, acting as discrete loads equivalent to a quasi-uniform pressure. Loading was performed in a stepwise manner with gradual load increase and holding periods at each stage until stabilization of the measured responses. All sandbags were weighed in advance using crane scales, and the applied loads are summarized in Table 1. The bags were distributed uniformly over the curved surface of the shell (loaded area A = 2.968 m²).

At the first loading step, 14 sandbags with a total weight of 0.62 t were placed, corresponding to a distributed load of 2.05 kN/m². The bags were initially arranged along the outer perimeter, providing partial surface coverage. At the second step, an additional 10 bags were placed to fully cover the shell surface. Thus, 24 sandbags with a total weight of 0.924 t were applied, equivalent to 3.05 kN/m².

At each subsequent step, 12 sandbags were added, resulting in 36, 48, 60, 72, 84, 96, and 108 bags at loading steps 3 to 9, respectively (see Table 1). At the penultimate step (step 10), 15 additional sandbags were placed, while at the final step (step 11), two concrete blocks with a total weight of 1.395 t were added. The total applied load on the specimen reached 6.13 t, corresponding to 20.25 kN/m².

After reaching the final loading stage, the shell was maintained under constant load for 2 h, after which the final readings of all measuring instruments were recorded. Selected loading stages are shown in Fig. 2, and the stepwise load increments are summarized in Table 1.

The shell was supported on a rigid test frame with plan dimensions of 2.2 × 2.2 m, fabricated as a spatial steel structure from rolled steel angles (L100 × 8 mm). The specimen was installed on the frame through its support ring to reproduce continuous contour support conditions.

Table 1 – Stepwise loading scheme of the structure

Step	Amount/type of applied load	Appled mass, t	Distributed load, kN/m^2
1	14 sandbags	0.620	2.05
2	24 sandbags	0.924	3.05
3	36 sandbags	1.386	4.58
4	48 sandbags	1.848	6.11
5	60 sandbags	2.310	7.63
6	72 sandbags	2.772	9.16
7	84 sandbags	3.234	10.69
8	96 sandbags	3.969	13.11
9	108 sandbags	4.158	13.74
10	113 sandbags	4.735	15.65
11	113 sandbags + 2 blocks	6.130	20.25

Figure 2 – Selected stages of structural loading

Measurement System

To monitor the deformation behavior of the 3DCP shell during loading, a combined measurement system was employed, consisting of strain gauges and mechanical dial displacement gauges (type 6PAO).

Relative strains were recorded using resistive strain gauges with a 20 mm gauge length, which were bonded to the inner surface of the shell at five characteristic locations. The strain gauge signals were collected using a multi-channel data acquisition system VNP-8 and transmitted to a personal computer for recording and processing.

Vertical deflections of the shell were measured using six mechanical dial gauges (6PAO) with a measurement accuracy of 0.01 mm. The gauges were directly attached to the shell surface. The layout of the strain gauges and deflection gauges is shown in Fig. 3, while the general view of the measurement equipment is presented in Fig. 4.

a) *b)*

Figure 3 – Layout of the measuring instruments: a) – deflection gauges, b) – strain gauges

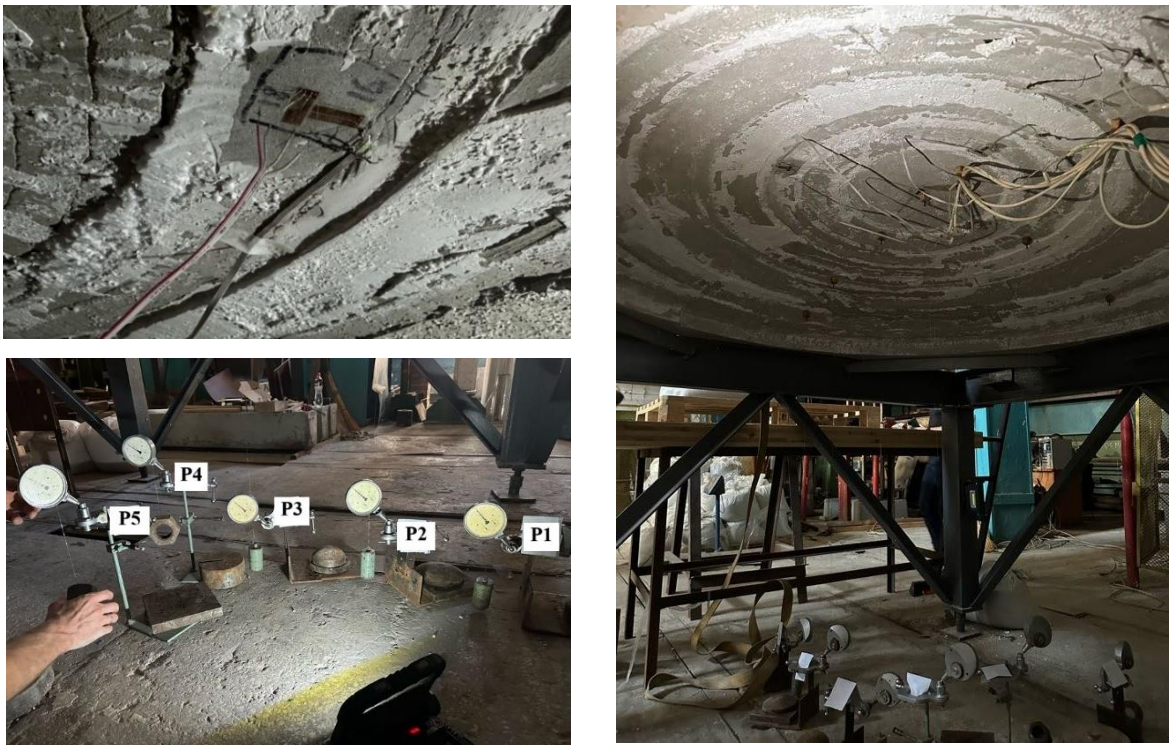

Figure 4 – General view of the measurement system (strain gauges and deflecrion gauges)

Experimental Results. Quantitative and qualitative assessment of the shell's vertical deflections was performed using 6PAO dial gauges, and the results are presented in Fig. 5. All load–deflection curves exhibit a nonlinear character: deflections increase more rapidly at low load levels (steps 1–2), while the rate of increase decreases at higher loads. Analysis of the load–deflection relationships within the investigated load range indicates a quasi-linear global structural response without abrupt changes in slope, which confirms the preservation of overall stiffness and the absence of progressive loss of load-bearing capacity within the measured range.

The maximum deflections in the central zone did not exceed 0.24 mm under a distributed load of 13.74 kN/m². At the same load level, isolated hairline cracks were visually observed in the support regions; however, these cracks did not exhibit further opening with subsequent load increments. This behavior is interpreted as a localization of stresses in the edge zones (support ring, contact with the test frame, and geometric imperfections), while the main portion of the shell continued to operate predominantly under a membrane-dominated mechanism within the tested load regime.

The obtained results confirm the sufficient spatial stiffness and efficiency of the adopted structural scheme of the shell.

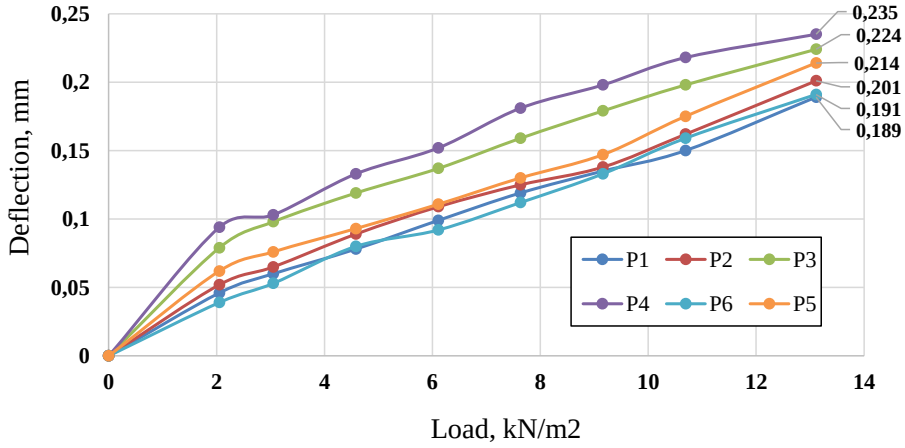

Figure 5 – Load–deflection relationship for the shell

Figure 6 – Appearance of hairline cracks in the support zones under a load of 13.74 kN/m²

Finite Element Analysis of the Stress–Strain State. To simulate the experimental behavior of the specimen, the LS-DYNA solver [19], implemented within the ANSYS Workbench environment, was employed. The numerical investigation of the 3D-printed concrete shell subjected to mechanical loading was performed in two stages.

At the first stage, the experimentally applied loading protocol was reproduced numerically. The main objective of this stage was to verify the numerical results by direct comparison with the experimental data.

At the second stage, the response of the 3D-printed concrete shell was analyzed under progressive mechanical loading up to the onset of failure.

To achieve a realistic representation of the stress-strain state, the boundary conditions were defined to reproduce the fixation of the shell on the experimental test frame. The concrete behavior was described using a continuous surface cap model (CSCM, material type No. 159 in LS-DYNA), as developed by Murray, Abu-Odeh, and Bligh [20].

The reinforcing steel was modeled using the PLASTIC KINEMATIC material model (type No. 003). The support frame was represented by a separate component assigned an ideal rigid material (MAT_RIGID, type No. 020).

Figure 7 shows the structural model of the test specimen together with the main element of the test setup – the support frame. Figure 8 illustrates the distributed loading scheme and the applied boundary conditions.

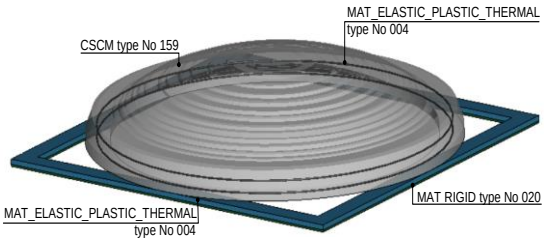

Figure 7 – Mapping of material models to the components of the reinforced concrete shell numerical model

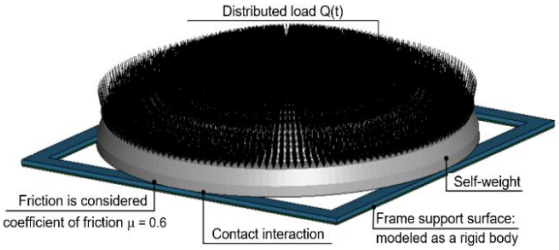

Figure 8 – Loading scheme and boundary conditions of the reinforced concrete shell

To assess the adequacy of the obtained numerical results, a comparative analysis with the experimental data was performed. Figures 9–10 present the experimental and numerical curves of displacements (according to Fig. 3a) and relative strains (according to Fig. 3b) of the shell under loading. Analysis of the data shown in Figs. 9–10 indicates good agreement between the experimental and numerical displacement values. This confirms that the developed mathematical model of the monolithic reinforced concrete dome element is adequate and capable of reliably reproducing the structural response.

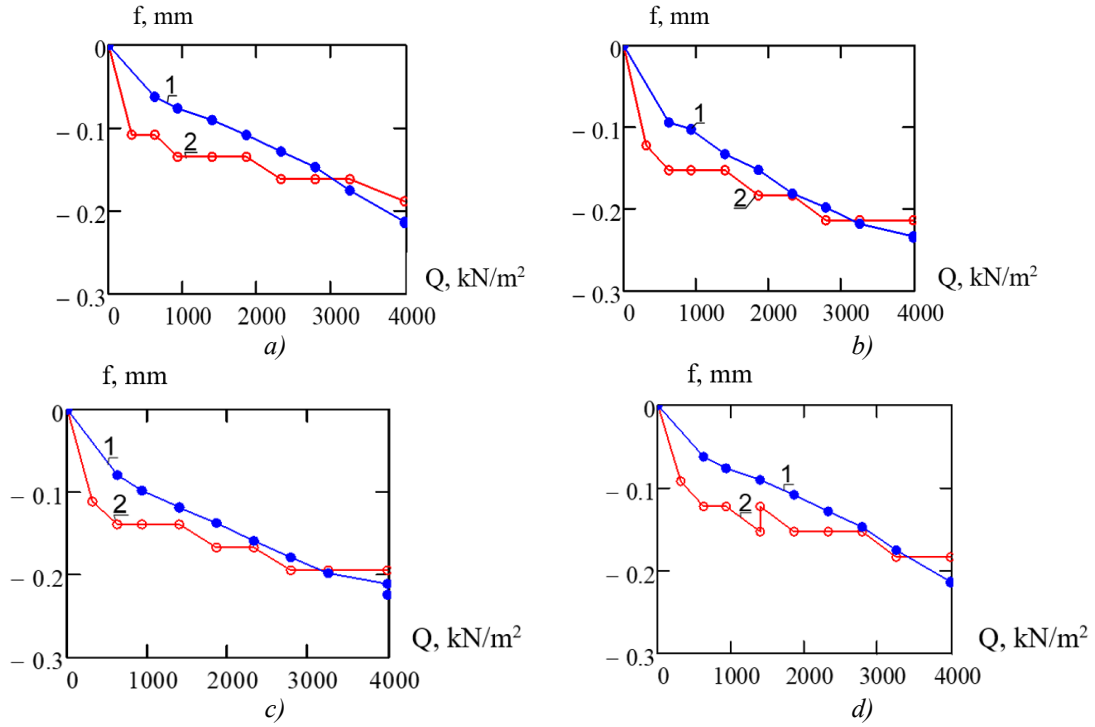

Figure 9 – Experimental (1) and numerical (2) displacement curves of the 3DCP shell at control points: a) – point P5; b) – point P4; c) – point P3; d) – point P6

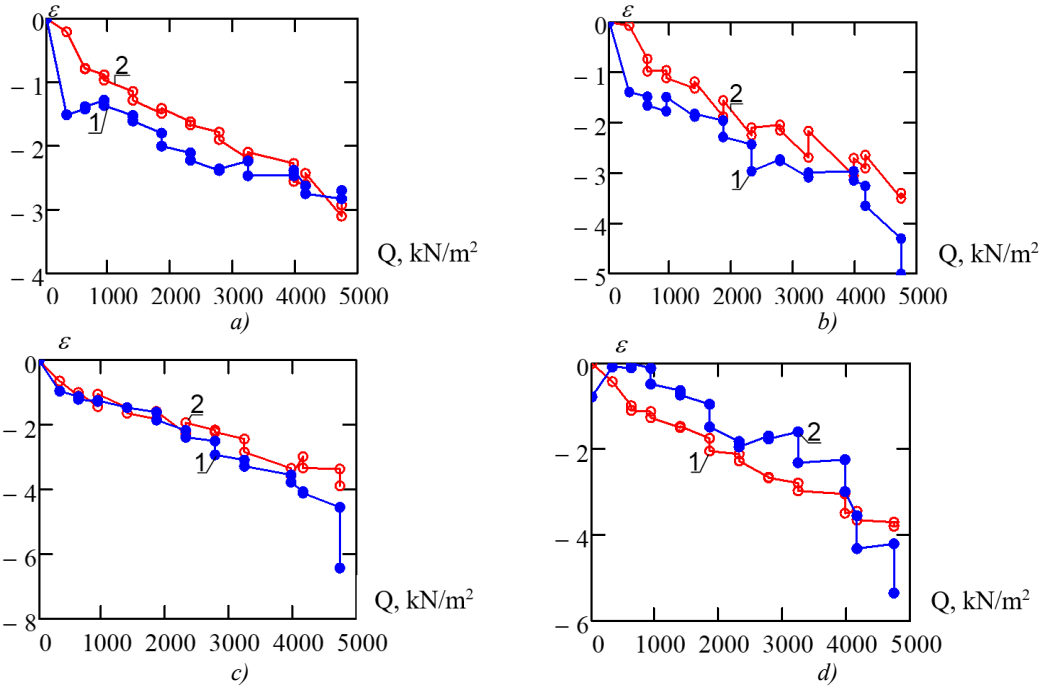

Figure 10 – Experimental (1) and numerical (2) relative strain curves at the control points of the 3DCP shell: a) – control points T12 and T14; b) – control points T16 and T18; c) – control points T6 and T8; d) – control points T0 and T2

The deviations between the experimental and numerical results were also analyzed. To verify the accuracy of the numerical predictions, the mean absolute, relative, and root-mean-square errors were calculated (Table 2).

Table 2 – Values of statistical indicators

Indicator	Absolute deviation	Relative deviation, %	Root mean square deviation
Maximum deflection of the top surface	0.025 mm	17.6	0.022 mm
Transverse displacement of the midpoint of the side wall	2.503×10^{-5}	16.9	2.102×10^{-5}

To investigate the failure conditions of the monolithic 3DCP shell, the numerical model was subjected to a gradual increase in load until signs of failure appeared. To track the onset of the ultimate limit state, the displacement curve of the highest point on the inner surface of the shell was constructed (Fig. 11). The behavior of this curve makes it possible to identify the state corresponding to structural failure. This state is associated with the onset of progressive (runaway) growth of displacements at points belonging to the analyzed element.

Four characteristic points on this curve, denoted by the letters A, B, C, and D, are highlighted in Fig. 11. The main parameters of these points and their descriptions are presented in Table 3.

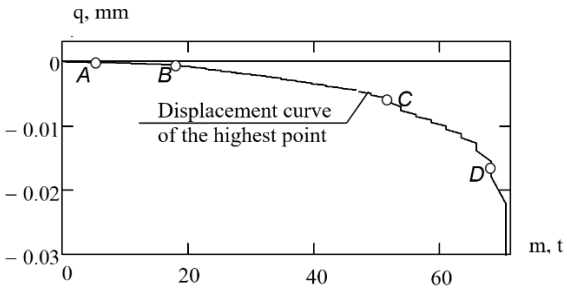

Figure 11 – Displacement curve of the highest point of the inner shell surface

Table 3 – Description of the characteristic points of the shell displacement curve

Characteristic point	Load Q, kN/m^2	Applied mass m, t	Displacement, mm	Description
A	2.0650	6.1289	-0.275	Characteristic point at which the experimental loading conditions are reproduced. At this point on the displacement curve, the onset of minor plastic deformations is observed in the tensile zone near the support surface. Small cracks may initiate.
B	68.600	20.360	-0.885	Characteristic point at which significant plastic deformations develop in the regions where the shell support surface does not contact the test frame. Cracks propagate along the shell generatrix at locations equidistant from the contact zones between the shell support surface and the frame. The displacement curve exhibits a noticeable change in slope with an increased rate of displacement growth.
C	172.500	51.198	-5.768	Development of significant plastic deformations and a branched crack system covering the entire shell area. The displacement curve shows a pronounced change in slope with an increased rate of displacement growth
D	228.400	67.789	-18.005	The displacement curve exhibits a sharp change in slope with runaway growth of displacements. This point is identified as the onset of complete structural failure of the shell.

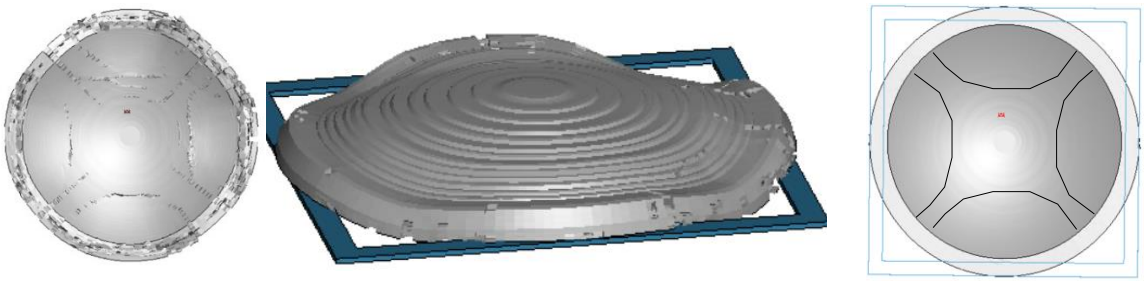

a) *b)*

Figure 12 – Failure pattern of the shell element (a) and schematic layout of the main cracks (b)

Based on the images shown in Fig. 12, the failure mechanism of the 3DCP shell under uniformly distributed loading and the adopted support conditions can be described as the formation of distinct segments bounded by main (primary) cracks. These segments become mobile once the yield limit of the reinforcing bars is reached, which leads to complete structural failure, as illustrated in Fig. 13.

Overall, the tested specimen demonstrates a high load-bearing capacity, as failure occurs under a uniformly distributed load of 228.4 kN/m², which corresponds to a total applied mass of 67.789 t.

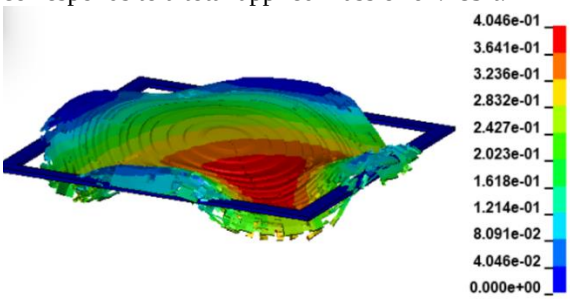

Figure 13 - Complete failure pattern of the test specimen with the vertical displacement field (m)

Conclusions.

The analysis of modern experimental methods for testing concrete shells showed that stepwise loading using artificial weights is an effective approach for evaluating their load-bearing capacity. The use of sandbags enables simulation of quasi-uniformly distributed pressure and realistic service loading conditions for shell structures.

The developed loading program provided reliable experimental data on shell deflections and strains. It was established that the maximum vertical displacements occur in the central zone (P4) and reach 0.235 mm under a load of 13.74 kN/m², indicating sufficient spatial stiffness of the tested element.

The three-dimensional finite element model accurately reproduces the stress–strain behavior of the shell. Comparison between numerical and experimental results confirmed its adequacy, with an average discrepancy in deflections not exceeding 17%.

The crack formation pattern and failure mechanism of the shell were investigated. Failure was found to occur progressively through the formation of main cracks in zones of maximum tensile stresses, after which individual shell segments lose stability.

The ultimate limit states and load-bearing capacity of the 3D-printed concrete shell were determined. The failure load reached 228.4 kN/m², corresponding to a total applied load of approximately 67.8 t, confirming the high structural potential of additively manufactured concrete shells.

The tested specimen, both as a geometric concept and as a technological demonstration of 3D concrete printing, shows strong potential for compression-dominated elements requiring high stiffness at minimal thickness. However, scaling to larger spans requires separate numerical justification due to the dependence of membrane forces on the shell radius.

The obtained results confirm the feasibility of using extrusion-based 3D concrete printing for producing thin-walled shells of complex geometry. The proposed experimental and numerical methodology can be recommended for further research and practical design of similar structures.

References

1. Reznik, P., Lugchenko, O., Volodymyrov, A., Tenesesku, V., Dzhamaldii, A., & Buldakov, O. (2025). Numerical analysis of 3D printed permanent formwork for reinforced concrete. *Collection of Scientific Works of the Ukrainian State University of Railway Transport*, 82–100. https://doi.org/10.18664/1994-7852.212.2025.336411
2. Surehali, S., Tripathi, A., & Neithalath, N. (2023). Anisotropy in additively manufactured concrete specimens under compressive loading—Quantification of the effects of layer height and fiber reinforcement. *Materials, 16*(15), 5488. https://doi.org/10.3390/ma16155488
3. Wolfs, R. J. M., Bos, F. P., & Salet, T. A. M. (2019). Hardened properties of 3D printed concrete: The influence of process parameters on interlayer adhesion. *Cement and Concrete Research, 119*, 132–140. https://doi.org/10.1016/j.cemconres.2019.01.009
4. Ding, T., Xiao, J., Zou, S., & Zhou, X. (2020). Anisotropic behavior in bending of 3D printed concrete reinforced with fibers. *Composite Structures, 254*, 112808. https://doi.org/10.1016/j.compstruct.2020.112808
5. Demchyna, B., Vozniuk, L., Surmai, M., Burak, D., & Shcherbakov, S. (2024). 3D printing technology for monolithic beams with the possibility of reinforcing bars. *Bulletin of Lviv National Environmental University. Series: Architecture and Construction, 25*, 32–37. https://doi.org/10.31734/architecture2024.25.032

1. Reznik, P., Lugchenko, O., Volodymyrov, A., Tenesesku, V., Dzhamaldii, A., & Buldakov, O. (2025). Numerical analysis of 3D printed permanent formwork for reinforced concrete. *Collection of Scientific Works of the Ukrainian State University of Railway Transport*, 82–100. https://doi.org/10.18664/1994-7852.212.2025.336411
2. Surehali, S., Tripathi, A., & Neithalath, N. (2023). Anisotropy in additively manufactured concrete specimens under compressive loading—Quantification of the effects of layer height and fiber reinforcement. *Materials, 16*(15), 5488. https://doi.org/10.3390/ma16155488
3. Wolfs, R. J. M., Bos, F. P., & Salet, T. A. M. (2019). Hardened properties of 3D printed concrete: The influence of process parameters on interlayer adhesion. *Cement and Concrete Research, 119*, 132–140. https://doi.org/10.1016/j.cemconres.2019.01.009
4. Ding, T., Xiao, J., Zou, S., & Zhou, X. (2020). Anisotropic behavior in bending of 3D printed concrete reinforced with fibers. *Composite Structures, 254*, 112808. https://doi.org/10.1016/j.compstruct.2020.112808
5. Demchyna, B., Vozniuk, L., Surmai, M., Burak, D., & Shcherbakov, S. (2024). 3D printing technology for monolithic beams with the possibility of reinforcing bars. *Bulletin of Lviv National Environmental University. Series: Architecture and Construction, 25*, 32–37. https://doi.org/10.31734/architecture2024.25.032

6. Zeng, J.-J., Yan, Z.-T., Jiang, Y.-Y., & Li, P.-L. (2024). 3D printing of FRP grid and bar reinforcement for reinforced concrete plates: Development and effectiveness. *Composite Structures*, *335*, 117946. https://doi.org/10.1016/j.compstruct.2024.117946
7. Zhang, D., Feng, P., Zhou, P., Xu, W., & Ma, G. (2023). 3D printed concrete walls reinforced with flexible FRP textile: Automatic construction, digital rebuilding, and seismic performance. *Engineering Structures*, *291*, 116488. https://doi.org/10.1016/j.engstruct.2023.116488
8. Chen, Y., Zhang, Y., Pang, B., et al. (2022). Steel fiber orientational distribution and effects on 3D printed concrete with coarse aggregate. *Materials and Structures*, *55*, 100. https://doi.org/10.1617/s11527-022-01943-7
9. Surianinov, M., Astafiev, D., Pidgorna, I., Volkov, A., & Baydalinov, A. (2023). Experimental study of long reinforced concrete cylindrical shells subjected to distributed loading. In *Progress in Engineering Sciences* (pp. 1–8). Trans Tech Publications. https://doi.org/10.32347/2076-815x.2023.83.314-324
10. Meza-de Luna, M., Rodríguez, A., & Torres, J. (2024). Experimental Study of Innovative FRC Dome-Shaped Structures with Industrial, Recycled, and Alternative Reinforcing under Compressive Load. *Ingeniería e Investigación, 44*(1). https://doi.org/10.15446/ing.investig.105266
11. Du, W., Zhu, L., Zhang, H., Zhou, Z., Wang, K., & Uddin, N. (2023). Experimental and Numerical Investigation of an Innovative 3DPC Thin-Shell Structure. *Buildings*, *13*(1), 233. https://doi.org/10.3390/buildings13010233
12. López, D., Bernat-Maso, E., Saloustros, S., Gil, L., Roca, P. (2023). Experimental testing and structural analysis of composite tile – reinforced concrete domes, *Engineering Structures*, *292*, *116512*, https://doi.org/10.1016/j.engstruct.2023.116512
13. Yemelyanova, T., & Lobanova, T. (2021). Stress–strain behavior of reinforced concrete cylindrical tanks under hydrostatic loading: Experimental validation. *Construction and Civil Engineering*, *1*, 42–52. https://doi.org/10.32851/tnv-tech.2021.1.7
14. Gaponova, L. V., Kalmykov, O. A., & Grebenchuk, S. S. (2015). Experimental–theoretical research of the stress–strain state of a spherical shell covering. *Collection of Scientific Works of UkrDUZT*, *157*, 102–113. https://doi.org/10.18664/1994-7852.157.2015.61641
15. Tenesesku, V. (2025). Technological aspects of fabricating a reinforced concrete shell using 3D concrete printing. *Building Constructions: Theory and Practice*, 17(4), 141–152. https://doi.org/10.32347/2522-4182.17.2025.141-152
16. Reznik, P., Volodymyrov, A., Maksymenko, V., & Alatayev, D. (2025). Strength anisotropy of 3D-printed concrete: Experimental investigation and statistical analysis. *Scientific Bulletin of Construction*, *112*. https://doi.org/10.33042/2311-7257.2025.112.1.30
17. Henkel Bautechnik Ukraine. (2024, October 3). *Ceresit 3D mixture testing protocol* (Laboratory report, 2 pp.).
18. Shmukler, V. S., Chuprynin, A. A., & Abbasi, R. (2009). Device for full-scale testing of slabs and shells (Ukrainian utility model patent No. 44125).
19. LS-DYNA. (2025). *LS-DYNA official website*. https://lsdyna.ansys.com/
20. Murray, Y. D., Abu-Odeh, A., & Bligh, R. (2006). *Evaluation of concrete material model 159* (FHWA-HRT-05-063). Federal Highway Administration.

6. Zeng, J.-J., Yan, Z.-T., Jiang, Y.-Y., & Li, P.-L. (2024). 3D printing of FRP grid and bar reinforcement for reinforced concrete plates: Development and effectiveness. *Composite Structures*, *335*, 117946. https://doi.org/10.1016/j.compstruct.2024.117946
7. Zhang, D., Feng, P., Zhou, P., Xu, W., & Ma, G. (2023). 3D printed concrete walls reinforced with flexible FRP textile: Automatic construction, digital rebuilding, and seismic performance. *Engineering Structures*, *291*, 116488. https://doi.org/10.1016/j.engstruct.2023.116488
8. Chen, Y., Zhang, Y., Pang, B., et al. (2022). Steel fiber orientational distribution and effects on 3D printed concrete with coarse aggregate. *Materials and Structures*, *55*, 100. https://doi.org/10.1617/s11527-022-01943-7
9. Surianinov, M., Astafiev, D., Pidgorna, I., Volkov, A., & Baydalinov, A. (2023). Experimental study of long reinforced concrete cylindrical shells subjected to distributed loading. In *Progress in Engineering Sciences* (pp. 1–8). Trans Tech Publications. https://doi.org/10.32347/2076-815x.2023.83.314-324
10. Meza-de Luna, M., Rodríguez, A., & Torres, J. (2024). Experimental Study of Innovative FRC Dome-Shaped Structures with Industrial, Recycled, and Alternative Reinforcing under Compressive Load. *Ingeniería e Investigación, 44*(1). https://doi.org/10.15446/ing.investig.105266
11. Du, W., Zhu, L., Zhang, H., Zhou, Z., Wang, K., & Uddin, N. (2023). Experimental and Numerical Investigation of an Innovative 3DPC Thin-Shell Structure. *Buildings*, *13*(1), 233. https://doi.org/10.3390/buildings13010233
12. López, D., Bernat-Maso, E., Saloustros, S., Gil, L., Roca, P. (2023). Experimental testing and structural analysis of composite tile – reinforced concrete domes, *Engineering Structures*, *292*, *116512*, https://doi.org/10.1016/j.engstruct.2023.116512
13. Yemelyanova, T., & Lobanova, T. (2021). Stress–strain behavior of reinforced concrete cylindrical tanks under hydrostatic loading: Experimental validation. *Construction and Civil Engineering*, *1*, 42–52. https://doi.org/10.32851/tnv-tech.2021.1.7
14. Gaponova, L. V., Kalmykov, O. A., & Grebenchuk, S. S. (2015). Experimental–theoretical research of the stress–strain state of a spherical shell covering. *Collection of Scientific Works of UkrDUZT*, *157*, 102–113. https://doi.org/10.18664/1994-7852.157.2015.61641
15. Tenesesku, V. (2025). Technological aspects of fabricating a reinforced concrete shell using 3D concrete printing. *Building Constructions: Theory and Practice*, 17(4), 141–152. https://doi.org/10.32347/2522-4182.17.2025.141-152
16. Shmukler, V. S., Chuprynin, A. A., & Abbasi, R. (2009). Device for full-scale testing of slabs and shells (Ukrainian utility model patent No. 44125).
17. Reznik, P., Volodymyrov, A., Maksymenko, V., & Alatayev, D. (2025). Strength anisotropy of 3D-printed concrete: Experimental investigation and statistical analysis. *Scientific Bulletin of Construction*, *112*. https://doi.org/10.33042/2311-7257.2025.112.1.30
18. Henkel Bautechnik Ukraine. (2024, October 3). *Ceresit 3D mixture testing protocol* (Laboratory report, 2 pp.).
19. LS-DYNA. (2025). *LS-DYNA official website*. https://lsdyna.ansys.com/
20. Murray, Y. D., Abu-Odeh, A., & Bligh, R. (2006). *Evaluation of concrete material model 159* (FHWA-HRT-05-063). Federal Highway Administration.

Олена Петрова
Харківський національний університет міського господарства імені О.М. Бекетова
https://orcid.org/0000-0003-0683-9694

Владислав Тенесеску
Харківський національний університет міського господарства імені О.М. Бекетова
https://orcid.org/0000-0002-8168-7224

Дмитро Петренко
Харківський національний університет міського господарства імені О.М. Бекетова
https://orcid.org/0000-0002-8168-7224

Олексій Булдаков
Харківський національний університет міського господарства імені О.М. Бекетова
https://orcid.org/0009-0002-4663-7392

Аналіз напружено-деформованого стану пологої сферичної оболонки, виготовленої методом 3D-друку бетоном (3DCP)

Аннотація. У статті розглянуто напружено-деформований стан та несучу здатність пологої сферичної оболонки покриття, виготовленої методом екструзійного 3D-друку бетоном. Метою дослідження є встановлення деформативності оболонки при дії квазірівномірно розподіленого навантаження та числове прогнозування її граничної несучої здатності на основі верифікованої скінченно-елементної моделі.
Об'єктом дослідження є оболонка діаметром 2.2 м, зі стрілою підйому 0.3 м та фактичною товщиною 80 мм, армована по опорному кільцю стрижнями Ø10 A500C. Навантаження створювалося ступінчасто шляхом укладання мішків із піском, рівномірно розподілених по площі оболонки (2.968 м²). Максимальне експериментальне навантаження становило 20.25 кН/м², що відповідало сумарній масі 6.13 т. Вертикальні переміщення вимірювалися механічними прогиномірами, а відносні деформації — тензометричними датчиками. Отримано, що максимальний прогин у центральній зоні досяг 0,235 мм при навантаженні 13,74 кН/м², що свідчить про високу просторову жорсткість оболонки.
Побудовану тривимірну скінченно-елементну модель у ПК LS-DYNA було верифіковано за експериментальними даними; розбіжність не перевищила 17 %. Числовим шляхом встановлено, що руйнування оболонки настає при навантаженні 228.4 кН/м², що відповідає сумарній вазі 67.8 т. Отримані результати підтверджують ефективність застосування 3D-друку бетоном для оболонкових конструкцій.

Ключові слова: бетони 3D-друку (3DCP); міцність на розтяг при згині; просічно-витяжний лист; скінченно-елементне моделювання; незнімна опалубка.

*Адреса для листування E-mail: Vladislav.Tenesesku@kname.edu.ua

Надіслано до редакції:	30.10.2025	Прийнято до друку після рецензування:	18.11.2025	Опубліковано (оприлюднено):	26.12.2025

Suggested Citation:

APA style: Petrova, O., Petrenko, D., Tenesesku, V., & Buldakov, O. (2025). Stress-Strain State Analysis of a Shallow Spherical Shell Fabricated Using 3DCP. *Academic Journal Industrial Machine Building Civil Engineering*, *2*(65), 35–45. https://doi.org/10.26906/znp.2025.65.4210

DSTU style: Stress-Strain State Analysis of a Shallow Spherical Shell Fabricated Using 3DCP / O. Petrova et al. *Academic journal. Industrial Machine Building, Civil Engineering*. 2025. Vol. 65, iss. 2. P. 35–45. URL: https://doi.org/10.26906/znp.2025.65.4210.